Regular Article

THROMBOSIS AND HEMOSTASIS

Conformational activation and inhibition of von Willebrand factor by targeting its autoinhibitory module

Nicholas A. Arce,[1] Zoe Markham-Lee,[2] Qian Liang,[1,3] Shabir Najmudin,[2] Emily R. Legan,[1] Gabrielle Dean,[1] Ally J. Su,[1] Moriah S. Wilson,[1] Robert F. Sidonio,[1] Pete Lollar,[1] Jonas Emsley,[2] and Renhao Li[1]

[1]Aflac Cancer and Blood Disorders Center, Children's Healthcare of Atlanta, Department of Pediatrics, Emory University School of Medicine, Atlanta, GA; [2]Biodiscovery Institute, School of Pharmacy, University of Nottingham, Nottingham, United Kingdom; and [3]Department of Laboratory Medicine, Ruijin Hospital, Shanghai Jiaotong University School of Medicine, Shanghai, China

KEY POINTS

- Conformationally insensitive nanobodies activate VWF binding of platelets by disrupting its NAIM.

- Conformationally sensitive nanobodies inhibit VWF binding of platelets by stabilizing the AIM conformation that masks the GPIbα-binding site.

Activation of von Willebrand factor (VWF) is a tightly controlled process governed primarily by local elements around its A1 domain. Recent studies suggest that the O-glycosylated sequences flanking the A1 domain constitute a discontinuous and force-sensitive autoinhibitory module (AIM), although its extent and conformation remains controversial. Here, we used a targeted screening strategy to identify 2 groups of nanobodies. One group, represented by clone 6D12, is conformation insensitive and binds the N-terminal AIM (NAIM) sequence that is distal from A1; 6D12 activates human VWF and induces aggregation of platelet-rich plasma at submicromolar concentrations. The other group, represented by clones Nd4 and Nd6, is conformation sensitive and targets the C-terminal AIM (CAIM). Nd4 and Nd6 inhibit ristocetin-induced platelet aggregation and reduce VWF-mediated platelet adhesion under flow. A crystal structure of Nd6 in complex with AIM-A1 shows a novel conformation of both CAIM and NAIM that are primed to interact, providing a model of steric hindrance stabilized by the AIM as the mechanism for regulating GPIbα binding to VWF. Hydrogen-deuterium exchange mass spectrometry analysis shows that binding of 6D12 induces the exposure of the GPIbα-binding site in the A1 domain, but binding of inhibitory nanobodies reduces it. Overall, these results suggest that the distal portion of NAIM is involved in specific interactions with CAIM, and binding of nanobodies to the AIM could either disrupt its conformation to activate VWF or stabilize its conformation to upkeep VWF autoinhibition. These reported nanobodies could facilitate future studies of VWF functions and related pathologies.

Introduction

von Willebrand factor (VWF) is a multimeric plasma glycoprotein essential for primary hemostasis.[1] VWF can activate and capture platelets to initiate thrombus formation by sensing and responding to altered blood flow.[2] Once activated, the A1 domain of VWF becomes exposed and binds to the ligand-binding domain (LBD) of glycoprotein (GP)Ibα on the platelet surface. Circulating VWF multimers do not bind platelets, indicating that VWF is autoinhibited under normal flow conditions. The whereabouts of the autoinhibitory elements in VWF and their molecular nature have been under investigation. Contrary to prior beliefs, multimeric VWF in solution may not adopt a collapsed globular shape, and a critical force threshold for uncoiling the multimer may not exist.[3,4] Because global extension of a VWF multimer is not sufficient to activate VWF,[5]

the primary autoinhibitory element should be close to the A1 domain. A number of studies have demonstrated the importance of the O-glycosylated sequences flanking the A1 domain to its platelet-binding activity.[6-12] Once A1 and LBD bind together, these flanking sequences may also modulate the unusual mechanical response of the A1-LBD interaction under certain shear flow conditions,[13-15] adding another layer of complexity to the regulation of VWF activity.

Recent biophysical studies indicate that an autoinhibitory module (AIM) consisting of both N- and C-terminal A1-flanking sequences adopts a quasi-stable conformation that prevents A1 binding to LBD.[16-18] Application of tension around 20 pN, which is achieved when the VWF multimer is placed under high shear,[5] could disrupt the protection of the A1 domain by the AIM to enable A1 binding to LBD.[18] Such tension should not

affect the conformational integrity of the A1 domain, because A1 is encompassed by a disulfide bond (Cys1272-Cys1458) that would require a rupture force of >100 pN.[19] Consistent with the notion of a discontinuous AIM, removal of either N- or C-terminal part of the AIM from the recombinant AIM-A1 protein significantly increases its binding affinity for LBD.[17,18] Moreover, introduction of type 2B von Willebrand disease mutations or desialylation of O-glycans in the AIM-A1 protein also destabilizes the AIM and increases the exposure of the GPIbα-binding site in the A1 domain.[18,20,21] The inhibitory nanobody that comprises caplacizumab, referred to as VHH81, binds primarily to N-terminal AIM (NAIM) residues proximal to the A1 domain and significantly increases the rupture force for the AIM,[18] suggesting that AIM may be a target for modulation of VWF activity.

Recent studies have disputed the notion of the discontinuous AIM.[22,23] The controversy may stem partly from how the A1 domain is defined. In this study and our earlier reports, the A1 domain is defined as residues encompassed by the 1272-1458 disulfide bond. Sequences outside the disulfide bond but resolved in the crystal structures, such as residues 1264-1271 and 1459-1469,[23] are not considered as a part of the A1 domain because they could be separated from A1 under tension, and they are not required for A1 binding to LBD.[18] Instead, we consider them as a part of the AIM, defined as NAIM (residues 1238-1271) and C-terminal AIM (CAIM; residues 1459-1493). In comparison, other groups consider these residues as a part of the A1 domain, because they interact noncovalently with residues inside of the 1272-1458 disulfide bond and help stabilize the A1 domain. Residues outside of 1264-1469 were considered only as "linker" sequences, implying a lack of stable conformation or specific interactions therein.[22,23] There are 8 O-glycans in the AIM or the "linker" sequences, at residues 1248, 1255, 1256, 1263, 1468, 1477, 1486, and 1487.[24,25] Previous mutagenesis analyses of O-glycosylation sites around the A1 domain have identified T1255A and T1255A/T1256A as activating mutations.[7,9] In addition, an activated VWF variant was generated when an unrelated O-glycosylated sequence was inserted between residues 1263 and 1264.[12] The "linker" region, including glycans therein, was thought as unstructured, and it "simply shields the A1 domain and reduces its accessibility to platelet GPIbα."[22] Thus, at the center of the controversy is the role of residues 1238-1260 (ie, the distal portion of the NAIM) in modulating the platelet-binding activity of VWF and whether these "linker" residues contain any specific interactions with themselves or residues in the A1 domain.

In this study, we conducted targeted screens for anti-AIM nanobodies, and we have identified both activating and inhibitory nanobodies. The characterization of these nanobodies provides evidence for the presence of specific interactions within residues 1238-1260 and for the conformational integrity of the AIM that determines the VWF activity.

Methods

Materials and animals
Monoclonal antibodies 6G1, CR1, and DNA aptamer ARC1172 have been described previously.[26,27] Ristocetin was purchased from MP Biomedicals and reconstituted to 25 mg/mL stocks in phosphate-buffered saline.

Recombinant protein expression and purification
Biotinylated VWF proteins AIM-A1 (residues 1238-1493), NAIM-A1 (1238-1461), A1-CAIM (1268-1493), tAIM-A1 (1261-1472), related variants, and GPIbα-LBD have been described previously.[18,28] VWF proteins Biotag-1238-1493-SpyTag, Biotag-1268-1493-SpyTag, and Biotag-1238-1461-SpyTag have been described previously.[18] The DNA fragment encoding Biotag-1261-1472-SpyTag was similarly cloned and expressed.[18] Constructs with a biotag (AviTag) were expressed from Expi293F BirA cells for biotinylation. Nonglycosylated AIM-A1 (Met-1238-1481-6His) was expressed in the cytoplasm of Shuffle T7 express cells (New England Biolabs). Nonglycosylated NAIM peptides with a N-terminal biotin group were synthesized by Genscript (supplemental Table 2, available on the *Blood* website). O-glycosylated NAIM peptides were expressed as Fc-fusion proteins in mammalian cells. Nanobodies were expressed in the cytoplasm of *Escherichia coli* and purified after cell lysis.[18]

Immunized yeast display library and targeted sorting
One adult *Lama glama* was immunized with the AIM-A1 protein by Abbiotec (Escondido, CA). Subsequently peripheral blood mononuclear cells were collected, from which complementary DNA of variable heavy domain of heavy chain (VHH) genes was amplified to construct a yeast display library. A library size of around 1.4×10^8 transformants was obtained from colony counts after serial dilutions of transformants. The library was initially enriched for AIM-A1 binding, then depleted with either NAIM-A1 or A1-CAIM, and again enriched for AIM-A1 binding (Figure 1). The details of this process are described in the supplemental Methods. Individual clones were then amplified and tested for their abilities to activate or inhibit the platelet-binding activity of VWF.

Platelet aggregometry
Written informed consent was obtained from participants before their inclusion in studies, and all procedures using donor-derived human blood and platelets were approved by the Institutional Review Board at Emory University. Platelet aggregation was performed largely as described.[18]

Biolayer interferometry
Biolayer interferometry experiments were performed on an Octet QK[e] instrument (ForteBio, Fremont, CA), largely as described previously.[5]

Hydrogen-deuterium exchange mass spectrometry (HDX-MS)
HDX-MS was performed largely as described.[21]

Parallel-plate flow chamber assay
Parallel-plate flow chamber experiments were performed using a Ibidi μ-Slide system. A tissue culture-treated Ibidi μ-Slide VI 0.1 device was coated with type 1 bovine collagen fibrils, and blocked with phosphate-buffered saline containing 1% bovine serum albumin. After citrated whole blood was mixed with 2 μg/mL DIOC-6 (Invitrogen), 2 mM $CaCl_2$, and various antagonists for 30 minutes, it was perfused at desired shear rates to the chamber using Harvard Apparatus Pump 11 Elite. A total of 3 to 4 images were captured along the center of the chamber at
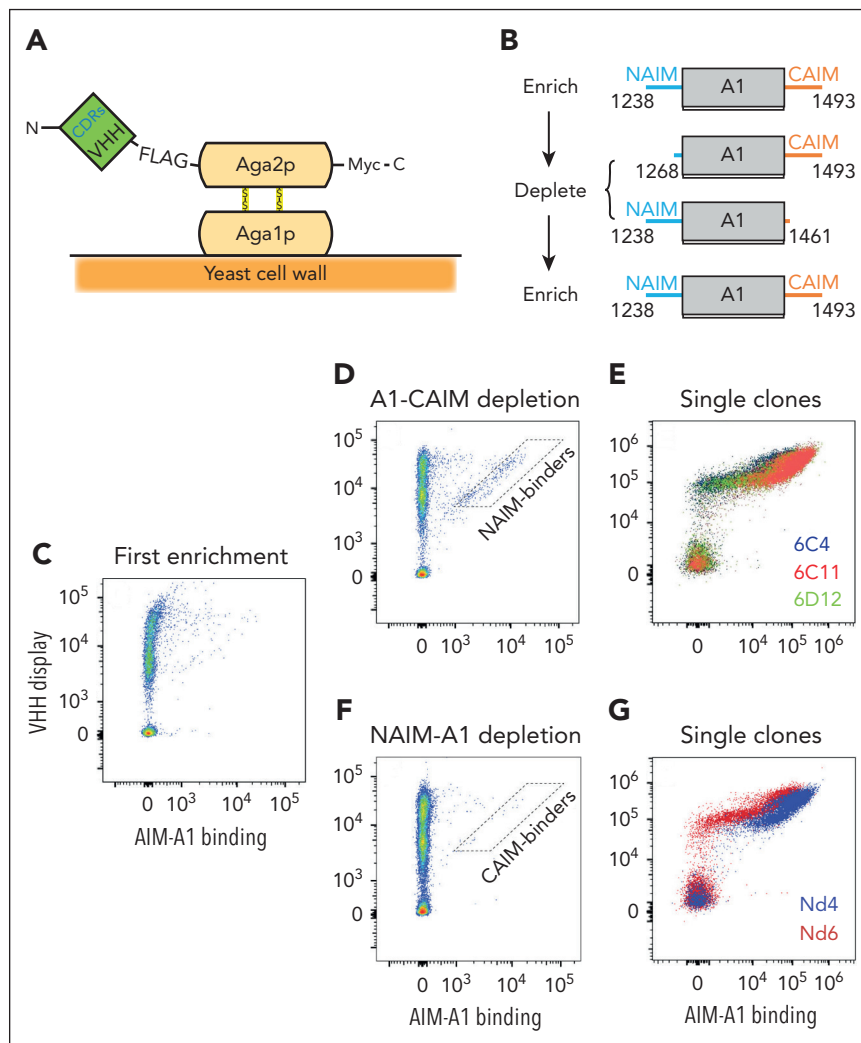
Figure 1. Screen of AIM-binding nanobodies by yeast surface display. (A) Schematic of the constructed yeast display library. Genes of VHH nanobodies were fused to that encoding the Aga2p subunit and VHH proteins were displayed on the yeast surface. (B) Schematic of the screening strategy. Yeasts were sorted for AIM-A1 binding, amplified, depleted with A1-CAIM or NAIM-A1 and re-sorted for AIM-A1 binding to obtain AIM-specific binders. Each protein is marked by the starting and ending VWF residues. (C-G) Flow cytometry plots showing binding of yeasts to AIM-A1 after various screening steps. In each plot, y-axis shows FLAG-tagged nanobody-Aga2p fusion protein expression on the yeast surface that is detected by Alexa Fluor 488-conjugated anti-FLAG antibody, and x-axis shows binding of the biotinylated AIM-A1 protein as detected by streptavidin-conjugated allophycocyanin. NAIM- and CAIM-specific binders were isolated from the approximate gates illustrated in the plots (D,F). After the second enrichment, individual clones (E,G) were isolated, amplified, and confirmed for AIM-A1 binding.

desired time points in the fluorescein-5-isothiocyanate (FITC) channel. Each experiment was performed in 2 separate flow channels at randomly nonconsecutive shear rates. Area covered by adhered platelets was calculated as described before.[18]

X-ray crystallography

The AIM-A1/nanobody complexes were purified and concentrated to ~16 mg/mL for crystallization. Crystals were harvested and 30% glycerol added as a cryo-protectant, then flash-frozen in liquid nitrogen for data collection on beamline i24 at Diamond Light Source. Diffraction data were collected from multiple crystals and processed to 3.05-Å resolution. The structure was solved using molecular replacement with the A1 domain crystal structure (1auq) and a nanobody model generated using AlphaFold.[29,30] Manual model building was performed using COOT and refinement with PHENIX/Refmac5/pdb-redo (Table 1). Figures were generated using PyMOL.

Additional details of the above methods, as well as those of enzyme-linked immunosorbent assay (ELISA), sodium dodecyl-sulfate polyacrylamide gel electrophoresis (SDS-PAGE), western blot, and dot blot can be found in the supplemental Methods.

Results

Nanobodies bind and activate human VWF

A llama was immunized with the AIM-A1 protein, and its VHH genes were amplified to construct a yeast display library (Figure 1). The initial 1.4×10^8 transformants of this library were enriched for binding to AIM-A1, depleted with binding to the NAIM-A1 or A1-CAIM protein, and then sorted again for binding to AIM-A1 (Figure 1B). From the screen with depletion by A1-CAIM, 3 anti-NAIM clones, designated 6C4, 6C11, and 6D12, were identified for their abilities to induce binding of AIM-A1 to recombinant LBD of GPIbα (Figure 1C-E). Only in the

Table 1. Data collection and structure refinement statistics

Sample	AIM-A1 Nd6 complex
Data collection	
Space group	P 1 2₁ 1
Cell dimensions	
a, b, c (Å)	38.8, 174.3, 197.3
α, β, γ (°)	90, 89.96, 90
Resolution (Å)*	65.8-3.05 (3.34-3.05)
R_{merge}†	0.709 (2.778)
R_{pim}†	0.0142 (0.573)
Total number unique	35 681 (1 758)
Mean(I)/sd(I)	5.4 (1.5)
Completeness (spherical) (%)	71.5 (15.0)
Completeness (ellipsoidal) (%)	89.9 (39.4)
Multiplicity	26.0 (23.1)
$CC^{1/2}$‡	0.984 (0.375)
Wavelength	0.9795
Refinement	
No. reflections	34 292
R_{work}§,*	0.234
R_{free}	0.297
Average B factor (Å²)	
AIM-A1 chains A/B/E/G/	85/89/74/75
Nd6 chains C/D/F/H/	50/50/47/43
4 × A2D A/B/E/G/	127/108/101/90
2 × CPS chains C/F	66/84
Solvent (75)	42
R.m.s. deviations	
Bond lengths (Å)	0.007
Bond angles (°)	1.604
Ramachandran statistics‖	
Favored (%)	85.9
Allowed (%)	9.4
Outliers (%)	4.7

R.m.s, root mean square; sd, standard deviation.

*Values in parentheses are for highest-resolution shell.

†R_{merge} = Sum(h) [Sum(j) [I(hj) − <Ih>]/Sum(hj) <Ih> where I is the observed intensity and <Ih> is the average intensity of multiple observations from symmetry-related reflections calculated.

‡$CC^{1/2}$ = Pearson correlation coefficient.

§R_{work} = Sum(h) ||Fo|h − |Fc|h|/Sum(h)|Fo|h, where Fo and Fc are the observed and calculated structure factors, respectively. R_{free} was computed as in R_{work}, but only for (5%) randomly selected reflections, which were omitted in refinement, calculated using REFMAC.

‖Ramachandran statistics were calculated using Molprobity.

presence of AIM-A1 could yeast cells displaying these nanobodies bind LBD (supplemental Figure 1).

Nanobodies 6C4, 6C11, and 6D12 were subcloned for bacterial overexpression, and purified nanobodies were monomeric (supplemental Figure 2). When added to stirred human platelet-rich plasma, all 3 nanobodies dose-dependently induced platelet aggregation, the extent of which matched that induced by 1.5 mg/mL ristocetin (Figure 2A-D). The aggregation was inhibited by DNA aptamer ARC1172 that targets the A1 domain[26] or antibody 11A8 that targets the LBD[16] (supplemental Figure 3), confirming that nanobody-induced aggregation was dependent on VWF and GPIbα. The half maximal effective concentration (EC₅₀) values for 6C4, 6C11, and 6D12 were ~167, ~100, and ~57 nM, respectively (Figure 2D). Consistently, binding of plasma VWF to immobilized LBD could be detected by ELISA but only in the presence of a nanobody (Figure 2E; supplemental Figure 4). Overall, these nanobodies could bind specifically to human VWF and induce its binding of GPIbα and activation of platelets.

## Activating nanobodies bind to a glycosylated distal sequence in NAIM

To define the mechanism by which these nanobodies activate human VWF, we characterized their binding epitopes. 6C4 bound with the lowest affinity (120 nM) among the 3 clones to AIM-A1. In comparison, 6C11 and 6D12 bound with tighter affinities at 14 and 31 nM, respectively (Figure 3A; supplemental Table 3). All 3 nanobodies exhibited binding to the NAIM-A1 protein but no detectable binding to A1-CAIM and tAIM-A1 (residues 1261-1472), confirming that these nanobodies target residues in the NAIM (Figure 3A;supplemental Figure 4C), likely residues preceding 1261.

Similar to monoclonal antibody 6G1,[27] all 3 nanobodies could recognize denatured AIM-A1 in western blot (Figure 3B), suggesting that they recognize a linear epitope in the NAIM. However, they could not recognize any 20-mer synthetic peptides covering the NAIM sequence on a dot blot, although they could recognize AIM-A1 on the same blot (Figure 3C), suggesting that their epitopes may contain an entity beyond the primary protein sequence.

The binding epitope of nanobody 6D12 was further defined. Recombinant AIM-A1 produced from Expi293F cells contains multiple O-linked core 1 glycans.[20] To test the hypothesis that the 6D12 epitope may include an O-glycan, nonglycosylated AIM-A1 protein was produced from E coli (supplemental Figure 5A-B). As expected,[27] antibody 6G1 exhibited the same binding to both glycosylated and nonglycosylated AIM-A1 (supplemental Figure 5C). In comparison, 6D12 bound only to glycosylated AIM-A1, with an apparent affinity of ~10 nM (Figure 3D). Next, human IgG1-Fc fusion proteins that contained the NAIM sequence (residues 1238-1271), or residues 1253-1266 that contained 3 O-glycosylation sites, were expressed from Expi293F cells (supplemental Figure 6A). 6D12 exhibited tight binding to both NAIM-Fc and 1253-1266–Fc, with binding affinities of 3.2 and 4.3 nM, respectively (Figure 3E; supplemental Figure 6B). Overall, these results demonstrate that the 6D12 epitope is in residues 1253-1266 of the NAIM and contains part of O-glycans therein. Consistently, activation of plasma VWF by 6D12 was not affected by the polymorphism at residue 1472 in the CAIM (supplemental Figure 7).

Binding of 6D12 exposes the GPIbα-binding site in the A1 domain

To analyze how 6D12 would activate A1, conformational dynamics of AIM-A1 with and without 6D12 binding was measured and compared by HDX-MS (Figure 4; supplemental
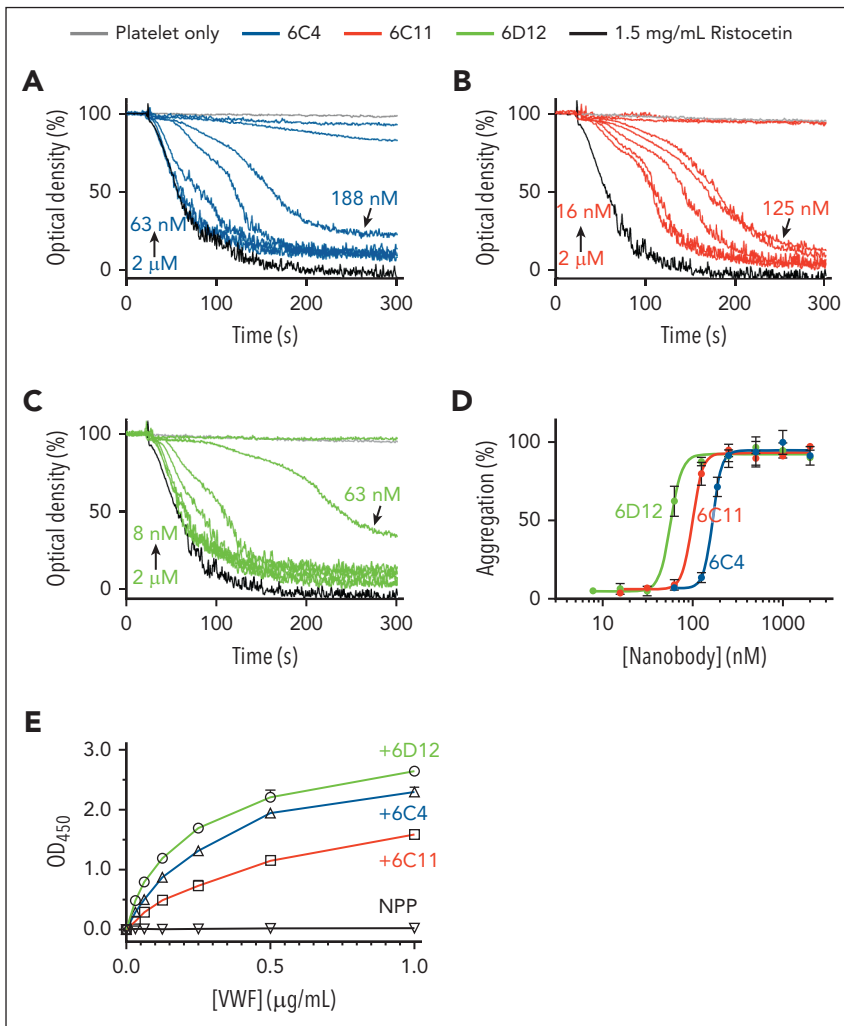
Figure 2. Activation of VWF by anti-NAIM nanobodies. (A-C) Platelet aggregation traces induced by addition of noted nanobodies. Human platelet-rich plasma was gently stirred, and, at 30 seconds, 6C4 (A), 6C11 (B), or 6D12 (C) was added to noted concentrations spanning from tens of nanomolar to 2 μM. Each concentration was tested in triplicate. Ristocetin was added in separate runs to 1.5 mg/mL, shown in black. Platelets stirred without addition of an agonist is shown in a gray trace. (D) Dose-aggregation curves were plotted for each concentration of each nanobody and fit to a 4-parameter dose-response curve. Percentage aggregation is the inverse of optical densities seen in panels A-C. Error bars are the standard deviation (SD) of the measurements. (E) ELISA binding isotherms of plasma VWF from normal pooled plasma (NPP) to immobilized GPIbα-LBD in the absence or presence of 500 nM noted nanobodies. Data are shown as mean ± SD (n = 3). Some error bars are not visible because they are smaller than the symbols.

Figures 8 and 9). A total of 121 peptic fragments were identified in both 6D12-bound and apo states of AIM-A1, covering ~97% of the sequence (supplemental Figure 8). A few fragments were identified covering VWF residues 1253-1266, but none exhibited substantial decrease in relative deuterium uptake (Figure 4B; supplemental Figure 8). This may be due to the inclusion of O-glycans in the 6D12 epitope. On the contrary, 6D12 binding increased HDX of several parts in the A1 domain, including particularly residues 1308-1313 (α1β2 loop) and 1328-1340 (β3α2 loop) that are a part of the GPIbα-binding site (Figure 4C-D). In addition, HDX of the nearby α3β4 loop (residues 1372-1378) was also significantly increased (Figure 4E). These results indicate that 6D12 binding increases the solvent accessibility of the GPIbα-binding site.

## Inhibition of VWF activity by anti-CAIM nanobodies

Two nanobodies, designated Nd4 and Nd6, were identified from the screen with depletion by NAIM-A1 to inhibit ristocetin-induced aggregation of human platelets (Figures 1F-G and 5A). In a parallel-plate flow chamber, both Nd4 and Nd6 significantly inhibited VWF-mediated platelet adhesion to collagen-coated surface under arterial shear rates (Figure 5B-C). Similar to that by nanobody VHH81, their inhibition was not complete, in that platelet adhesion was still visible at high shear rates. In

comparison, ARC1172, a DNA aptamer that directly inhibits the VWF-GPIbα interaction, achieved complete inhibition regardless of the shear rates. We showed earlier that VHH81 inhibits VWF binding to GPIbα indirectly by binding primarily to the proximal portion of the NAIM and stabilizing the AIM.[18] These results suggest that Nd4 and Nd6 likely inhibit VWF binding to GPIbα via a similar mechanism as VHH81.

Both Nd4 and Nd6 could bind to AIM-A1, albeit with disparate affinities of 19 and 600 nM, respectively (Figure 6A; supplemental Figure 10). Their binding specificity to CAIM was confirmed because neither nanobody exhibited binding to NAIM-A1. Both could bind to tAIM-A1 (residues 1261-1472) with similar affinities to AIM-A1, suggesting that their epitopes are proximal to A1. Unlike activating nanobodies described above, neither Nd4 nor Nd6 could detect AIM-A1 in dot blots, indicating that they target conformationally specific epitopes (Figure 6B). For comparison, antibody 6G1 that binds to residues 1461-1472 in the CAIM could blot AIM-A1, and CR1 that has a conformationally sensitive epitope could blot AIM-A1 weakly.[27]

Structural and dynamic characterization of the AIM-A1/Nd6 complex

The crystal structure of AIM-A1 in complex with Nd6 was determined to 3.0-Å resolution (supplemental Figures 11 and 12;
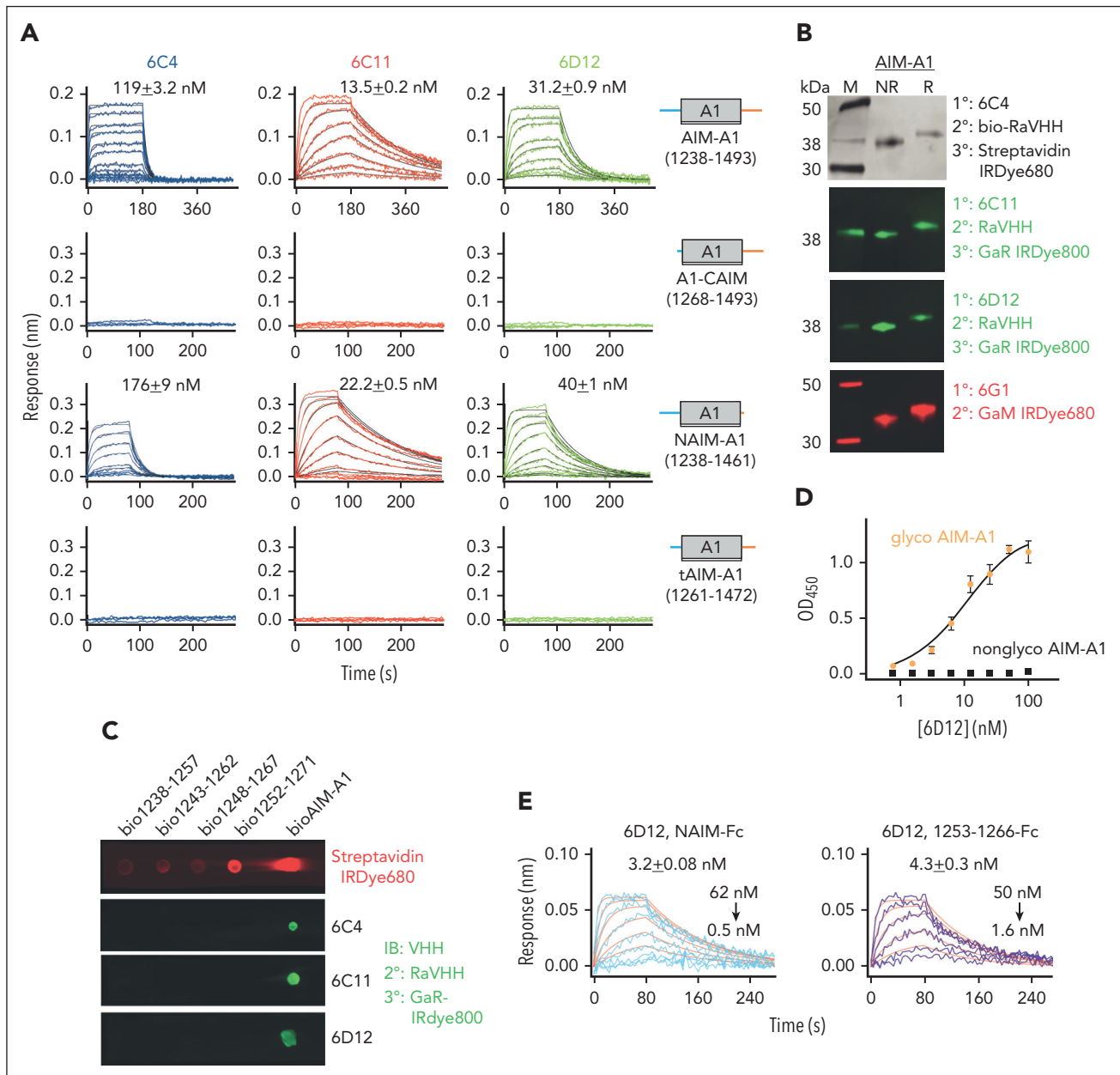
Figure 3. Identification of the epitopes of VWF-activating nanobodies. (A) Representative BLI sensorgrams of immobilized AIM-A1, A1-CAIM, NAIM-A1, or tAIM-A1 binding to a serial dilution of purified nanobody 6C4 (blue), 6C11 (red), or 6D12 (green). Nanobody concentration ranges are 2 µM to 2 nM for 6C4 binding to AIM-A1, 250 nM to 2 nM for 6C11 and 6D12 binding to AIM-A1, and 500 nM to 1 nM for all others. The fitted affinity, when obtained, is shown in each panel. For AIM-A1, association was performed for 180 seconds and dissociation for 360 seconds. For A1-CAIM, NAIM-A1, and tAIM-A1, association was performed for 80 seconds and dissociation for 200 seconds. The fitting trace for each concentration is shown in black. (B) Western blots of nonreduced (NR) or reduced (R) AIM-A1 with noted nanobody or antibody 6G1. To accommodate the fast off-rate of 6C4, a biotinylated rabbit anti-VHH antibody (bio-RaVHH) and streptavidin-IRDye680 were used to detect blotting of AIM-A1 by 6C4. After blotting with 6C11 and 6D12, a rabbit anti-VHH antibody (RaVHH) and fluorescent goat anti-rabbit antibody (GaR) were used to visualize the blots. 6G1 binds to a linear epitope in the CAIM, and it was detected using a fluorescent goat anti-mouse secondary antibody (GaM). (C) Dot blots of biotinylated NAIM peptides (10 ng per spot) and bio-AIM-A1 (1 µg per spot). Each membrane strip was blotted with noted nanobody separately and detected with RaVHH and fluorescent GaR. To verify proper adsorption of biotinylated peptides and bio-AIM-A1 protein to the strip, the same strip was blotted with streptavidin-IRDye680. (D) ELISA binding isotherms of 6D12 to immobilized glycosylated AIM-A1 purified from mammalian cells (orange circles) and nonglycosylated AIM-A1 purified from *E coli* (black squares). Data are shown as mean ± SD (n = 3). Responses were fit to a hyperbola and the K_D (10.7 ± 3.2 nM) was derived from half-maximal binding. (E) BLI binding traces of 6D12, in a dilution series, to immobilized NAIM-Fc, 1253-1266-Fc, and neuraminidase-treated NAIM-Fc (asialo-NAIM-Fc). Global kinetic fitting at ratio 1:1 is shown in red, and kinetic K_D is listed on top of the sensorgrams.

Figure 6C-E; Table 1). The AIM-A1/Nd4 complex was also prepared for crystallization (supplemental Figure 12), but the crystal contained only Nd4, likely due to the acidic crystallizing condition that may have disrupted the complex (data not shown). In the Nd6 complex structure, VWF residues 1263 to 1472 were resolved, including the O-linked N-acetylgalactosamine on

residue 1468 (Figure 6C-D). Nd6 interacts with the proximal portion of the CAIM and some residues from the A1 domain. Specifically, the Nd6 Ile29 main chain nitrogen and Tyr33 side chain hydroxyl form hydrogen bonds with Glu1434 of VWF, and the Nd6 His34 side chain forms a water-mediated hydrogen bond with the main chain of Asp1459 of VWF (Figure 6D-E).
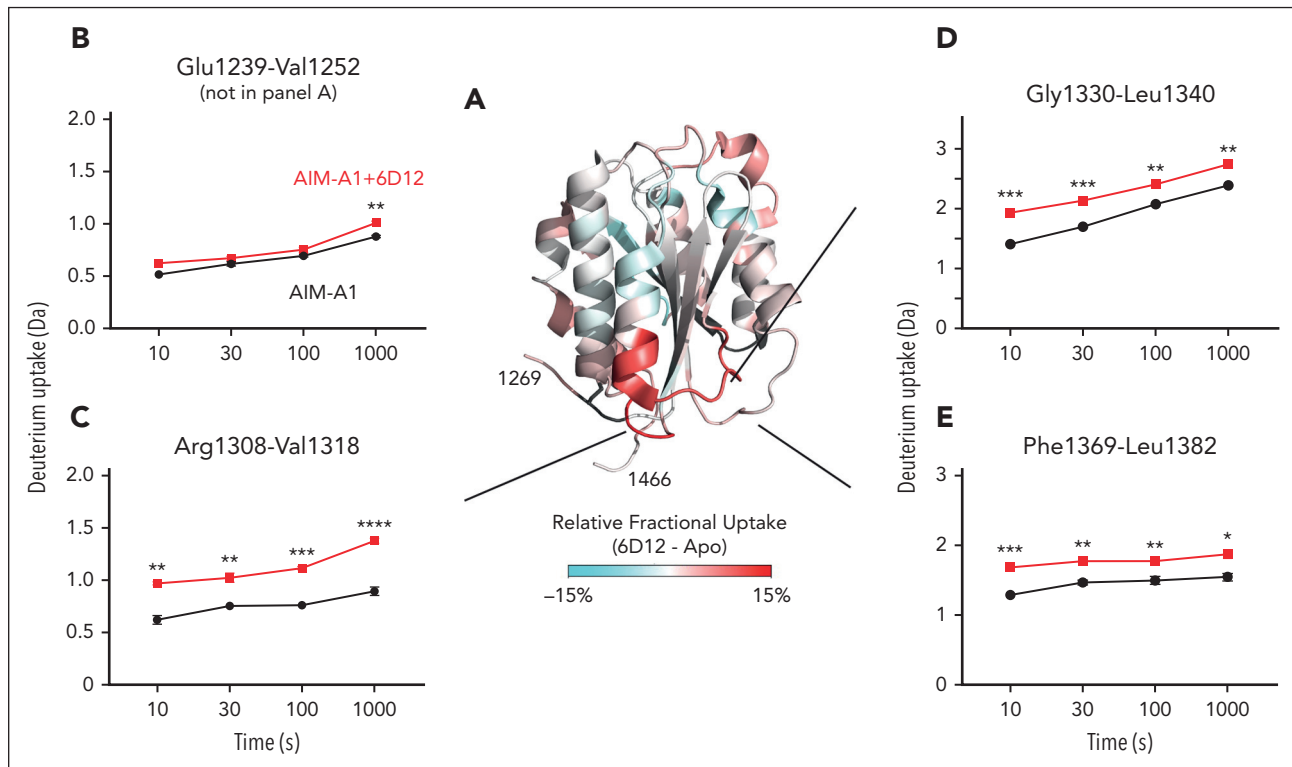
Figure 4. Comparative HDX of AIM-A1 protein with and without bound 6D12. (A) Relative deuterium uptake displayed on the 3D structure of the A1 domain and partial AIM (PDB 1SQ0). Residues experiencing more exchange in the presence of 6D12 are colored in shades of red, no difference in exchange is displayed as white, and decreased exchange is shown in cyan. Note that many residues in the AIM were unresolved in this structure. (B-E) Uptake plots of representative peptides in AIM-A1 with (red) and without (black) bound 6D12 at 10, 30, 100, and 1000 seconds of exchange. Peptide 1239-1252 (B) is a NAIM-peptide. Peptide 1308-1318 (C) is in the α1β2 loop of the A1 domain, peptide 1330-1340 (D) is in the β3α2 loop, and peptide 1369-1382 (E) is in the α3β4 loop. For each time point, experiments were performed in triplicate. ****$P < .0001$ using a Student t test; ***$P < .001$; **$P < .01$; *$P < .05$.

In addition, there is a hydrogen bond interaction formed by Nd6 Ser55 side chain hydroxyl and the Ala1464 main chain carbonyl of VWF, and a long-range salt bridge formed by Asp78 of Nd6 and Lys1408 of VWF. The rest of interactions between VWF and Nd6 are van der Waals contacts, consistent with the relatively weak binding affinity between Nd6 and AIM-A1.

HDX of AIM-A1 in complex with equal molar Nd6 was measured and compared with apo-AIM-A1. A total of 104 peptic fragments were identified in both states of AIM-A1 (supplemental Figures 13 and 14). Binding of Nd6 reduced HDX of several parts in the AIM-A1 protein, including residues in the NAIM, α1β2, β3α2, and α3β4 loops (Figure 6F-J). This is opposite of the effects induced by 6D12 binding (Figure 4). Binding of Nd4 and VHH81 exhibited similar reducing effects on the same regions (supplemental Figures 15 and 16), suggesting that these inhibitory nanobodies stabilize the AIM and reduce the exposure of the GPIbα-binding site.

A comparison of Nd6 and VHH81 complex structures[18] reveals that the A1 domain structure is indistinguishable (Figure 7A). Although Nd6 and VHH81 bind to drastically different epitopes in AIM-A1, AIM residues in these 2 structures take on similar conformations, which suggests that both nanobodies stabilize the same conformation of the AIM. In contrast, 2 major differences are apparent between AIM-A1 structures in their complexes with Nd6 and LBD.[31-33] One lies in the α1β2 loop (supplemental Figure 17). The other, larger difference lies in the AIM, both in terms of

resolved residues and their conformations (Figure 7B-C). When superimposed together, CAIM residues and the α1β2 loop in the Nd6 complex would overlap in space with the N-terminal residues in the LBD, illustrating the structural basis for Nd6 inhibition.

Discussion

In this study, a screen of nanobodies that specifically target the AIM instead of the A1 domain produced both activators and inhibitors of VWF (Figures 1, 2, and 5). All activating nanobodies are conformationally insensitive, and their epitopes were mapped to an O-glycosylated sequence in the NAIM that is distal to the A1 domain (Figure 3). Binding of the representative clone 6D12 induces the exposure of the GPIbα-binding site in the A1 domain (Figure 4). On the contrary, both inhibitory nanobodies are conformationally sensitive, and their epitopes include residues in the CAIM (Figure 6). Their binding reduces the exposure of the GPIbα-binding site (Figure 6). The AIM-A1/Nd6 complex structure resolves the most CAIM residues among all reported A1 structures, and these residues would overlap with bound GPIbα, suggesting that Nd6 binding stabilizes the AIM conformation to prevent A1 binding to GPIbα. Taken together, our results support a model for VWF autoinhibition and activation in which conformational stability of the AIM determines the platelet-binding activity of VWF (Figure 7D). In this model, NAIM and CAIM residues together form the AIM. The AIM masks the GPIbα-binding site but not the β3 strand in the A1 domain, which could be strengthened by VWF inhibitors or disrupted by activators. Similar
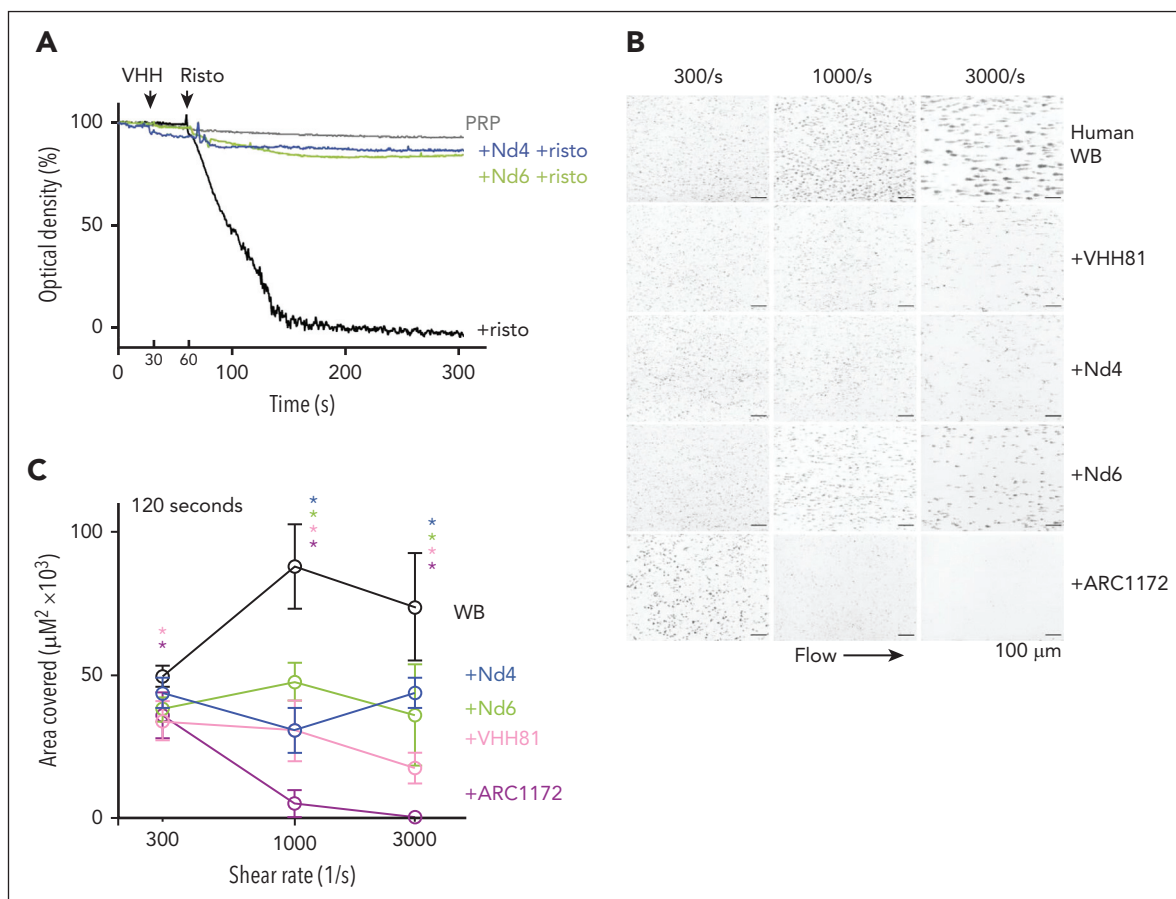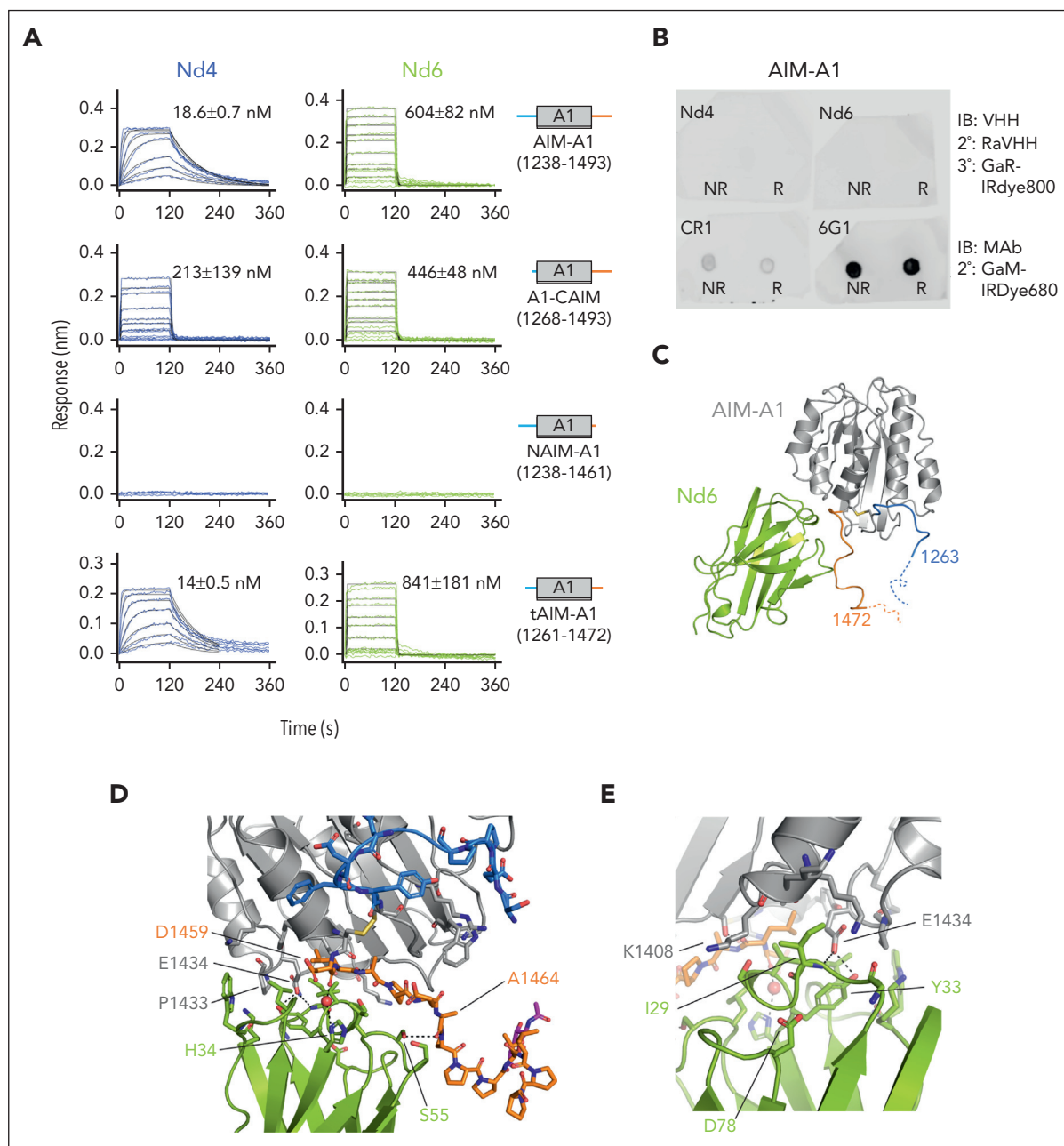
Figure 5. Nanobodies Nd4 and Nd6 inhibit the activity of human VWF. (A) Ristocetin-induced platelet aggregation traces with or without the addition of 1 μM Nd4 or Nd6. Human platelet-rich plasma (PRP) was gently stirred with addition of each nanobody at 30 seconds, followed by addition of 1.5 mg/mL ristocetin at 60 seconds. (B) Representative flow chamber surface images at 120 seconds of human whole blood perfusion on collagen. Recalcified whole blood labeled with DIOC-6 was mixed with noted nanobody or aptamer inhibitors and then perfused over a collagen surface at given shear rates. The scale bar is 100 μm. Platelet adhesion was measured by thresholding pixel densities to calculate the area covered by adherent platelets. (C) Quantitative plots of platelet adhesion on collagen under noted shear rates and with treatment of various inhibitors (Nd4 in blue, Nd6 in green, VHH81 in pink, and ARC1172 in purple). Comparison between platelet adhesion was analyzed with a 2-way ANOVA with mixed effects with Tukey multiple comparison correction. Asterisks in given colors represent statistically significant values ($P < .0001$) between control blood and individual treatments at a given shear rate after multiple comparison corrections. Data are means ± SD (n = 8-12 fields analyzed per condition). Interaction $F_{(8, 142)} = 26.31$; $P < .0001$; shear rate $F_{(2, 142)} = 7.47$; $P = .0008$; treatment $F_{(4, 142)} = 141.7$; $P < .0001$. ANOVA, analysis of variance.

to Nd6, VHH81 is also conformationally sensitive and inhibits VWF, although it binds primarily NAIM residues (Figure 7A).[18] Similar to 6D12, 6G1 is a conformationally insensitive antibody that could activate the AIM-A1 protein.[18] Unlike 6D12, 6G1 binds a linear epitope in the proximal portion of the CAIM.[27]

A key observation of the AIM-A1/Nd6 complex structure is that, although no direct contacts were observed between Nd6 and VWF residues 1465-1472, residues 1467-1472 were resolved for the first time in a crystal structure. Resolved residues of NAIM and CAIM point toward each other and away from the A1 domain (Figure 7A-C), likely placing some unresolved residues in the structure in the same vicinity for interaction with each other. The adoption of a specific conformation or interaction by the unresolved residues, especially 1253 to 1263 including the associated glycans, is supported by our discovery of activating nanobodies. If residues 1238-1260 did not contain a structural element and were only to provide hindrance as a "linker" sequence, attaching a sizable nanobody such as 6D12 to this stretch of residues would only increase its hindrance on GPIbα binding. However 6D12 binding clearly activates VWF and exposes its GPIbα-binding site.

Our result is consistent with earlier reports that mutations at residues 1255 and/or 1256 could activate VWF.[7,9]

That NAIM and CAIM residues point toward each other has not been observed in previously reported structures of the A1 domain.[26,29,31-41] Except for complex structures of A1 with LBD and AIM-A1 with VHH81,[18,31] all previous A1 structures used nonglycosylated proteins produced from bacteria.[26,29,32-41] In the first A1/LBD complex structure, a yeast-expressed protein containing residues 1261-1468 and bearing the R1306Q mutation was used, thus without the distal portion of the NAIM.[31] The AIM-A1/VHH81 structure used the same glycosylated AIM-A1 protein as in the Nd6 complex structure,[18] but not as many CAIM residues were resolved, presumably without stabilization of the CAIM by Nd6. Desialylation, particularly that of O-glycans around the A1 domain, contributes to VWF activation.[20,42] Thus, a bacterial-expressed nonglycosylated A1 protein may not contain a sufficiently stable AIM. It may also support a nonnative conformation in the crystal structure. For instance, in the unbound A1 structure,[29] the side chain of Ser1263 was pointing toward the A1 domain. If the residue was O-glycosylated as in its

Figure 6. Epitopes of inhibitory nanobodies Nd4 and Nd6. (A) Representative BLI sensorgrams of immobilized AIM-A1, A1-CAIM, NAIM-A1, or tAIM-A1 binding to a serial dilution of purified nanobody Nd4 (blue) or Nd6 (green). Nanobody concentration ranges are 64 to 1 nM for Nd4 binding to AIM-A1, tAIM-A1, 4 µM to 2 nM for Nd4 binding to A1-CAIM, 20 µM to 20 nM for Nd6 binding to AIM-A1, A1-CAIM and tAIM-A1, and 2 µM to 125 nM for Nd4 and Nd6 binding to NAIM-A1. The fitted affinity, when obtained, is shown in each panel. For binding, association was performed for 120 seconds, and dissociation for 240 seconds. The fitting trace for each concentration is shown in black. (B) Dot blots of immobilized NR and R AIM-A1 by Nd4 and Nd6. 6G1, which recognizes a linear epitope, and CR1, which is partially conformationally sensitive, were included for comparison. (C) Crystal structure of the AIM-A1/Nd6 complex, shown in ribbon diagram. The nanobody Nd6 is shown in green, the A1 domain in gray, NAIM residues in sky blue, and CAIM residues in orange. Dashed lines denote unresolved residues in AIM-A1. (D-E) Close-up diagrams showing specific contacts between AIM-A1 and Nd6. Hydrogen bonds between side chains or main chains of noted residues are marked by dashed lines. Note that CAIM residues beyond residue Ala1464 do not show any direct contacts with Nd6. The GalNAC group on residue 1468 is colored magenta. (F) Relative deuterium uptake displayed on the 3D structure of the A1 domain and partial AIM as in the Nd6 complex. Residues experiencing more exchange in the presence of Nd6 are colored in shades of red, no difference in exchange is displayed as white, and decreased exchange is shown in cyan. Note that many residues in the AIM were unresolved in this structure. (G-J) Uptake plots of representative peptides in AIM-A1 with (green) and without (black) bound 6D12 at 10, 30, 100, and 1000 seconds of exchange. Peptide 1240-1257 (G) is a NAIM-peptide. Peptide 1308-1320 (H) is in the α1β2 loop of the A1 domain, peptide 1330-1340 (I) is in the β3α2 loop, and peptide 1367-1383 (J) is in the α3β4 loop. For each time point, experiments were performed in triplicate. ***$P < .001$ using a Student t test; **$P < .01$; *$P < .05$.

native form, its pointing toward A1 would have created steric hindrance. Several cryoEM structures of D1-A1 domains have been reported to model the packed VWF tubule in the Weibel-Palade body.[43,44] Although proteins in these structures were produced from mammalian cells, they contain no CAIM residues beyond residue 1464. Neither structures show resolved NAIM residues before 1263.[43,44] The E3 module in the D'D3 assembly that adjoins the NAIM is not resolved in these structures.
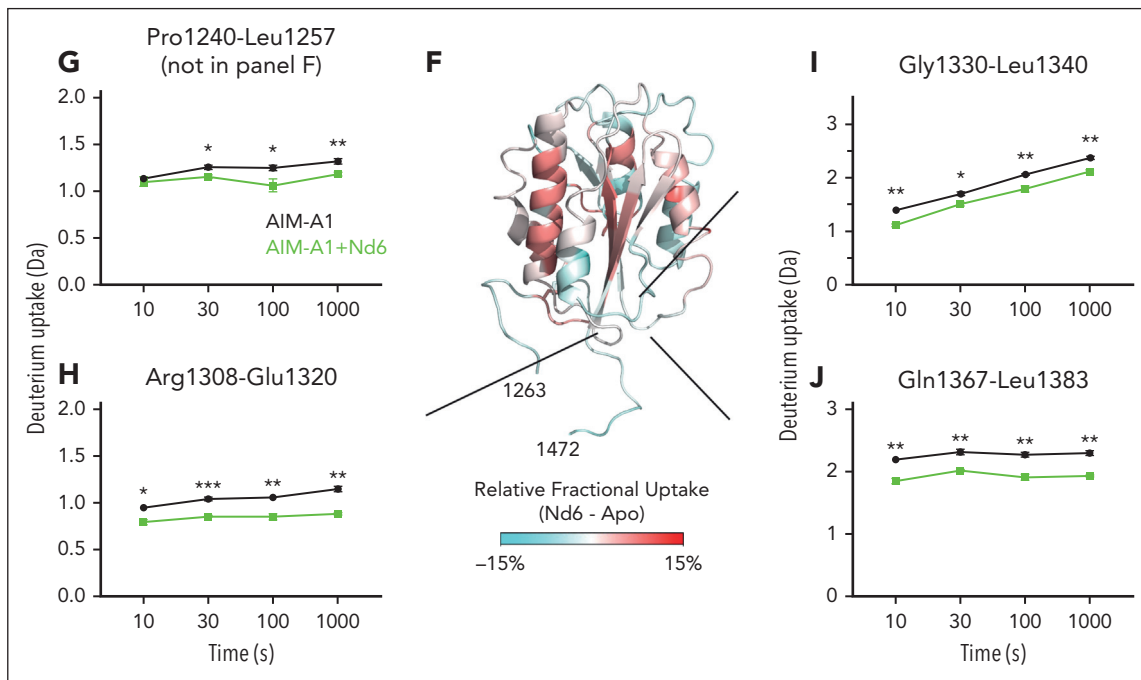
ARCE et al

Figure 6 (continued)

Despite stabilization by Nd6, the distal portion of the AIM, including O-glycans therein, is not resolved in the Nd6 complex structure. This is possibly due to the heterogeneity of O-glycans in the AIM. Although the AIM-A1 protein contains primarily core 1 O-glycans, both monosialylated and disialylated forms with either α-2,3 or α-2,6 linkage are present.[20] At the present time, there are no effective means to generate the AIM-A1 protein with homogeneous O-glycans. The specific interactions

Figure 7. Comparison of the Nd6 complex structure with other A1 structures suggests a model of VWF auto-inhibition and activation. (A) Overlaid Nd6 and VHH81 complex structures, with resolved AIM residues zoomed in and highlighted in the box on the right. Nd6 is shown in green, VHH81 in pink, and both AIM-A1 in gray. Resolved NAIM and CAIM residues from the Nd6 structure are shown in sky blue and orange, respectively. Resolved NAIM and CAIM residues from the VHH81 structure are shown in light purple and yellow, respectively. (B) Ribbon diagram of the A1/LBD complex structure (PDB: 1sq0), with the resolved AIM residues highlighted in purple and magenta. (C) Overlaid Nd6 and LBD complex structures, showing only AIM-A1 from the Nd6 complex structure and LBD from the LBD complex structure. The highlight box on the right shows the overlap of resolved AIM residues with the N-terminus of the LBD. (D) Illustration of the AIM model of VWF autoinhibition and activation. A structured AIM would have steric hindrance with the LBD, thus shielding A1 from binding to LBD. Conformationally insensitive nanobodies, such as 6D12 and 6C11, can bind to the NAIM residues distal from the A1 domain and disrupt the AIM, which exposes A1 for binding to the LBD. Conversely, conformationally sensitive nanobodies such as Nd6 and VHH81 can bind and stabilize the AIM, thus inhibiting A1 binding to the LBD.
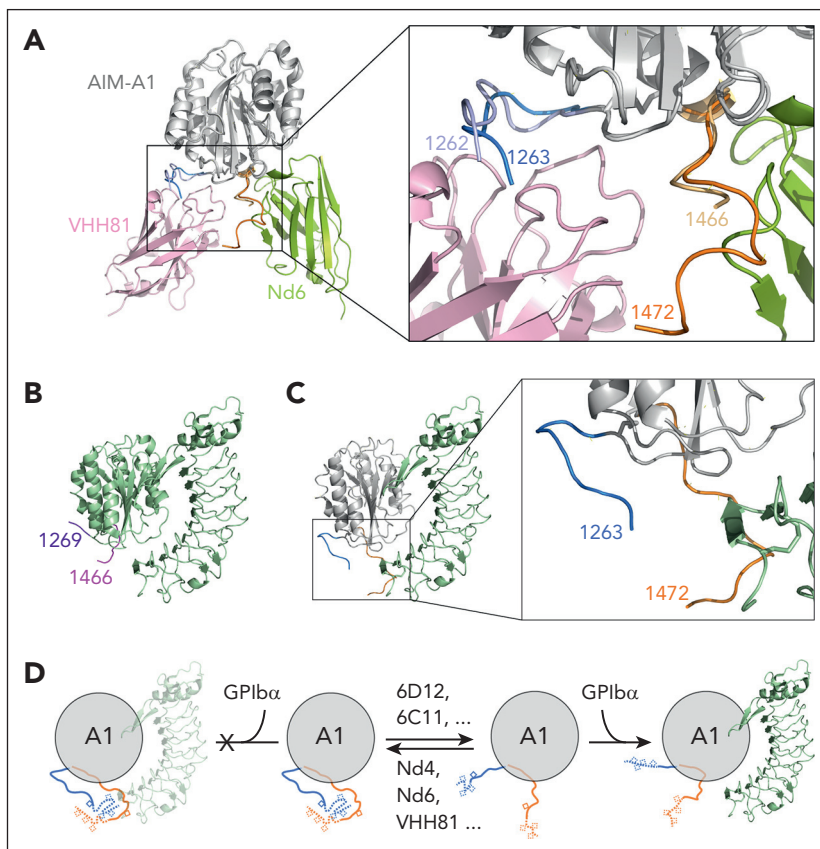
involving sialylated residues 1253-1266 remain to be determined.

It was suggested that hydrogen bonds between proximal NAIM residues (eg, 1264-1271) and the A1 domain are critical in keeping the latter in an inactive conformation and breaking them induces A1 to an active conformation primed for LBD binding.[23,45] Although proximal NAIM residues in Nd6 and VHH81 complex structures take on similar conformations (Figure 7A), they are sufficiently different to form different hydrogen bonds with A1. It is not apparent how different sets of hydrogen bonds between NAIM and A1 help upkeep the same autoinhibited state of A1.

Ristocetin is widely used as an activator of human VWF in research and diagnosis. The ristocetin-binding site in VWF include primarily the A1-proximal portion of the CAIM.[16] Ristocetin forms dimers when exceeding a concentration of 1.1 mg/mL, and dimeric ristocetin may facilitate VWF-dependent agglutination of platelets.[46] Ristocetin could also bind and flocculate many other plasma proteins such as fibrinogen.[46] Nanobody 6D12 is much more specific for VWF with a nano-molar affinity than ristocetin (Figure 3). Because 6D12 remains monomeric for all the concentrations used in this study (supplemental Figure 2), the ability of dimerization or oligomer-ization may not be required for an activator of VWF.

6D12 exhibits a higher affinity for NAIM-Fc and 1253-1266–Fc than it does for AIM-A1 protein (Figures 2 and 4), suggesting that its epitope in the NAIM is somewhat protected in AIM-A1. Relatedly, although 6C11 exhibits a higher binding affinity for AIM-A1 than 6D12, the latter is superior in inducing platelet aggregation with a lower EC_{50} value. Thus, additional factors in full-length VWF may affect the accessibility of the NAIM, and each nanobody may activate VWF to a different extent. Future studies are needed to elucidate the intrinsic efficacy of these nanobodies as VWF activators.

Several nanobodies have been developed to target VWF for various purposes. Nanobody AU/VWFa-11 binds preferentially to activated A1 domain of VWF than its inactive state, and it does not affect the VWF-GPIbα interaction.[47] Another nano-body with similar preferential binding to VWF containing type 2B von Willebrand disease mutations than wild-type VWF was reported recently.[48] The epitopes of these nanobodies were not reported, and it is unclear how they specifically recognize the GPIbα-binding state of the A1 domain. In addition, Aymé et al reported an inhibitory nanobody targeting the A1 domain, and it cross-reacted with both human and mouse VWF.[49] How it inhibits the A1 activity, by binding directly to the GPIbα-binding site or binding to the AIM like VHH81 and Nd6 do, is not clear. Kizlik-Masson et al developed a nanobody that binds the A3 domain, and its binding could be reduced by ADAMTS13 cleavage of the A2 domain nearby.[50] Recently, de Maat et al reported 2 nanobodies targeting the D'D3 assembly and the CT/CK domain, respectively, both of which were used in a fusion protein to facilitate protease cleavage of VWF multimers as potential therapeutics.[51] In this paper, we report several nanobodies, particularly 6D12, with an activating function. Compared with ristocetin, these nanobodies are monomeric,

highly specific to VWF, and their activation of VWF is not affected by common polymorphisms in VWF. They may be useful in future investigation and measurement of physiological and pathophysiological processes involving activated VWF.

Authorship

Contribution: N.A.A., J.E., and R.L. designed the study; N.A.A., Z.M.-L., Q.L., E.R.L., A.J.S., M.S.W., and P.L. performed experiments; G.D. and R.F.S. collected clinical samples; N.A.A., Z.M.-L., Q.L., S.N., E.R.L., P.L., J.E., and R.L. analyzed results and prepared figures; N.A.A. and R.L. wrote the manuscript; and Q.L., S.N., E.R.L., J.E., and P.L. edited the manuscript.

Conflict-of-interest disclosure: R.L., N.A.A., and Q.L. are inventors on pending patents describing VWF-modulating nanobodies and their uses. The remaining authors declare no competing financial interests.

ORCID profiles: N.A.A., 0000-0002-0019-0380; Z.M.-L., 0000-0002-8048-0926; Q.L., 0000-0003-3985-2633; S.N., 0000-0002-0429-5454; A.J.S., 0000-0001-6447-3438; M.S.W., 0000-0003-3687-0078; R.F.S., 0000-0002-9509-9415; P.L., 0000-0002-1206-8104; J.E., 0000-0002-8949-8030; R.L., 0000-0002-5806-5080.

Correspondence: Renhao Li, Department of Pediatrics, Emory University School of Medicine, 2015 Uppergate Drive NE, Room 440, Atlanta, GA 30322; email: renhao.li@emory.edu.

REFERENCES

1. Sadler JE. Biochemistry and genetics of von Willebrand factor. *Annu Rev Biochem*. 1998; 67:395-424.

2. Springer TA. von Willebrand factor, Jedi knight of the bloodstream. *Blood*. 2014; 124(9):1412-1425.

3. Parker ET, Lollar P. Conformation of the von Willebrand factor/factor VIII complex in quasi-static flow. *J Biol Chem*. 2021;296:100420.

4. Bergal HT, Jiang Y, Yang D, Springer TA, Wong WP. Conformation of von Willebrand factor in shear flow revealed with stroboscopic single-molecule imaging. *Blood*. 2022;140(23):2490-2499.

5. Fu H, Jiang Y, Yang D, Scheiflinger F, Wong WP, Springer TA. Flow-induced elongation of von Willebrand factor precedes tension-dependent activation. *Nat Commun*. 2017;8(1):324.

6. Auton M, Cruz MA, Moake J. Conformational stability and domain unfolding of the von Willebrand factor A domains. *J Mol Biol*. 2007;366(3):986-1000.

7. Badirou I, Kurdi M, Legendre P, et al. In vivo analysis of the role of O-glycosylations of von Willebrand factor. *PLoS One*. 2012;7(5): e37508.

8. Auton M, Sowa KE, Behymer M, Cruz MA. N-terminal flanking region of A1 domain in von Willebrand factor stabilizes structure of A1A2A3 complex and modulates platelet activation under shear stress. *J Biol Chem*. 2012;287(18):14579-14585.

9. Nowak AA, Canis K, Riddell A, Laffan MA, McKinnon TA. O-linked glycosylation of von Willebrand factor modulates the interaction with platelet receptor glycoprotein Ib under static and shear stress conditions. *Blood*. 2012;120(1):214-222.

10. Tischer A, Cruz MA, Auton M. The linker between the D3 and A1 domains of vWF suppresses A1-GPIbalpha catch bonds by site-specific binding to the A1 domain. *Protein Sci*. 2013;22(8):1049-1059.

11. Madabhushi SR, Zhang C, Kelkar A, Dayananda KM, Neelamegham S. Platelet GpIba binding to von Willebrand Factor under fluid shear:contributions of the D'D3-domain, A1-domain flanking peptide and O-linked glycans. *J Am Heart Assoc*. 2014;3(5):e001420.

12. Zhang C, Kelkar A, Nasirikenari M, et al. The physical spacing between the von Willebrand factor D'D3 and A1 domains regulates platelet adhesion in vitro and in vivo. *J Thromb Haemost*. 2018;16(3):571-582.

13. Yago T, Lou J, Wu T, et al. Platelet glycoprotein Ibalpha forms catch bonds with human WT vWF but not with type 2B von Willebrand disease vWF. *J Clin Invest*. 2008; 118(9):3195-3207.

14. Kim J, Zhang CZ, Zhang X, Springer TA. A mechanically stabilized receptor-ligand flex-bond important in the vasculature. *Nature*. 2010;466(7309):992-995.

15. Zhao YC, Wang HQ, Wang Y, Lou JZ, Ju LA. The N-terminal autoinhibitory module of the A1 domain in von Willebrand factor stabilizes the mechanosensor catch bond. *RSC Chem Biol*. 2022;3(6):707-720.

16. Deng W, Wang Y, Druzak SA, et al. A discontinuous autoinhibitory module masks the A1 domain of von Willebrand factor. *J Thromb Haemost*. 2017;15(9):1867-1877.

17. Deng W, Voos KM, Colucci JK, et al. Delimiting the autoinhibitory module of von Willebrand factor. *J Thromb Haemost*. 2018; 16(10):2097-2105.

18. Arce NA, Cao W, Brown AK, et al. Activation of von Willebrand factor via mechanical unfolding of its discontinuous autoinhibitory module. *Nat Commun*. 2021;12(1):2360.

19. Wiita AP, Ainavarapu SR, Huang HH, Fernandez JM. Force-dependent chemical kinetics of disulfide bond reduction observed with single-molecule techniques. *Proc Natl Acad Sci U S A*. 2006;103(19):7222-7227.

20. Voos KM, Cao W, Arce NA, et al. Desialylation of O-glycans activates von Willebrand factor by destabilizing its autoinhibitory module. *J Thromb Haemost*. 2022;20(1):196-207.

21. Legan ER, Liu Y, Arce NA, et al. Type 2B von Willebrand disease mutations differentially perturb autoinhibition of the A1 domain. *Blood*. 2023;141(10):1221-1232.

22. Tischer A, Machha VR, Moon-Tasson L, Benson LM, Auton M. Glycosylation sterically inhibits platelet adhesion to von Willebrand factor without altering intrinsic conformational dynamics. *J Thromb Haemost*. 2020;18(1):79-90.

23. Bonazza K, Iacob RE, Hudson NE, et al. von Willebrand factor A1 domain stability and affinity for GPIbalpha are differentially regulated by its O-glycosylated N- and C-linker. *Elife*. 2022;11:e75760.

24. Canis K, McKinnon TA, Nowak A, et al. The plasma von Willebrand factor O-glycome comprises a surprising variety of structures including ABH antigens and disialosyl motifs. *J Thromb Haemost*. 2010;8(1):137-145.

25. Solecka BA, Weise C, Laffan MA, Kannicht C. Site-specific analysis of von Willebrand factor O-glycosylation. *J Thromb Haemost*. 2016; 14(4):733-746.

26. Huang RH, Fremont DH, Diener JL, Schaub RG, Sadler JE. A structural explanation for the antithrombotic activity of ARC1172, a DNA aptamer that binds von Willebrand factor domain A1. *Structure*. 2009;17(11):1476-1484.

27. De Luca M, Facey DA, Favaloro EJ, et al. Structure and function of the von Willebrand factor A1 domain: analysis with monoclonal antibodies reveals distinct binding sites involved in recognition of the platelet membrane glycoprotein Ib-IX-V complex and ristocetin-dependent activation. *Blood*. 2000; 95(1):164-172.

28. Arce NA, Liu Y, Chen W, Zhang XF, Li R. Autoinhibitory module underlies species difference in shear activation of von Willebrand factor. *J Thromb Haemost*. 2022; 20(11):2686-2696.

29. Emsley J, Cruz M, Handin R, Liddington R. Crystal structure of the von Willebrand factor A1 domain and implications for the binding of platelet glycoprotein Ib. *J Biol Chem*. 1998;273(17):10396-10401.

30. McCoy AJ, Grosse-Kunstleve RW, Adams PD, Winn MD, Storoni LC, Read RJ. Phaser crystallographic software. *J Appl Crystallogr*. 2007;40(pt 4):658-674.

31. Huizinga EG, Tsuji S, Romijn RA, et al. Structures of glycoprotein Iba and its complex with von Willebrand factor A1 domain. *Science*. 2002;297(5584):1176-1179.

32. Dumas JJ, Kumar R, McDonagh T, et al. Crystal structure of the wild-type von Willebrand factor A1-glycoprotein Iba complex reveals conformation differences with a complex bearing von Willebrand disease mutations. *J Biol Chem*. 2004; 279(22):23327-23334.

33. Blenner MA, Dong X, Springer TA. Structural basis of regulation of von Willebrand factor binding to glycoprotein Ib. *J Biol Chem*. 2014;289(9):5565-5579.

34. Celikel R, Varughese KI, Madhusudan, Yoshioka A, Ware J, Ruggeri ZM. Crystal structure of the von Willebrand factor A1 domain in complex with the function blocking NMC-4 Fab. *Nat Struct Biol*. 1998;5(3):189-194.

35. Fukuda K, Doggett TA, Bankston LA, Cruz MA, Diacovo TG, Liddington RC. Structural basis of von Willebrand factor activation by the snake toxin botrocetin. *Structure*. 2002;10(7):943-950.

36. Maita N, Nishio K, Nishimoto E, et al. Crystal structure of von Willebrand factor A1 domain complexed with snake venom, bitiscetin: insight into glycoprotein Ibalpha binding mechanism induced by snake venom proteins. *J Biol Chem*. 2003;278(39):37777-37781.

37. Fukuda K, Doggett T, Laurenzi IJ, Liddington RC, Diacovo TG. The snake venom protein botrocetin acts as a biological brace to promote dysfunctional platelet aggregation. *Nat Struct Mol Biol*. 2005;12(2): 152-159.

38. Tischer A, Campbell JC, Machha VR, et al. Mutational constraints on local unfolding inhibit the rheological adaptation of von Willebrand factor. *J Biol Chem*. 2016;291(8): 3848-3859.

39. Zhu S, Gilbert JC, Hatala P, et al. The development and characterization of a long acting anti-thrombotic von Willebrand factor (VWF) aptamer. *J Thromb Haemost*. 2020; 18(5):1113-1123.

40. Celikel R, Ruggeri ZM, Varughese KI. von Willebrand factor conformation and adhesive function is modulated by an internalized water molecule. *Nat Struct Biol*. 2000;7(10): 881-884.

41. Lee HT, Park UB, Jeong TJ, et al. High-resolution structure of the vWF A1 domain in complex with caplacizumab, the first

nanobody-based medicine for treating acquired TTP. *Biochem Biophys Res Commun.* 2021;567:49-55.

42. Grainick HR, Williams SB, Coller BS. Asialo von Willebrand factor interactions with platelets. Interdependence of glycoproteins Ib and IIb/IIIa for binding and aggregation. *J Clin Invest.* 1985;75(1):19-25.

43. Anderson JR, Li J, Springer TA, Brown A. Structures of VWF tubules before and after concatemerization reveal a mechanism of disulfide bond exchange. *Blood.* 2022; 140(12):1419-1430.

44. Javitt G, Yeshaya N, Khmelnitsky L, Fass D. Assembly of von Willebrand factor tubules with in vivo helical parameters requires A1 domain insertion. *Blood.* 2022;140(26): 2835-2843.

45. Kim J, Hudson NE, Springer TA. Force-induced on-rate switching and modulation by mutations in gain-of-function von Willebrand diseases. *Proc Natl Acad Sci U S A.* 2015;112(15):4648-4653.

46. Scott JP, Montgomery RR, Retzinger GS. Dimeric ristocetin flocculates proteins, binds to platelets, and mediates von Willebrand factor-dependent agglutination of platelets. *J Biol Chem.* 1991;266(13): 8149-8155.

47. Hulstein JJ, de Groot PG, Silence K, Veyradier A, Fijnheer R, Lenting PJ. A novel nanobody that detects the gain-of-function phenotype of von Willebrand factor in ADAMTS13 deficiency and von Willebrand disease type 2B. *Blood.* 2005;106(9): 3035-3042.

48. van der Vorm LN, Li L, Huskens D, et al. Analytical characterization and reference interval of an enzyme-linked immunosorbent assay for active von Willebrand factor. *PLoS One.* 2019;14(2):e0211961.

49. Ayme G, Adam F, Legendre P, et al. A novel single-domain antibody against von Willebrand factor A1 domain resolves leukocyte recruitment and vascular leakage during inflammation-brief report. *Arterioscler Thromb Vasc Biol.* 2017;37(9):1736-1740.

50. Kizlik-Masson C, Peyron I, Gangnard S, et al. A nanobody against the von Willebrand factor A3-domain detects ADAMTS13-induced proteolysis in congenital & acquired VWD. *Blood.* 2023; 141(12):1457-1468.

51. de Maat S, Clark CC, Barendrecht AD, et al. Microlyse: a thrombolytic agent that targets VWF for clearance of microvascular thrombosis. *Blood.* 2022;139(4):597-607.
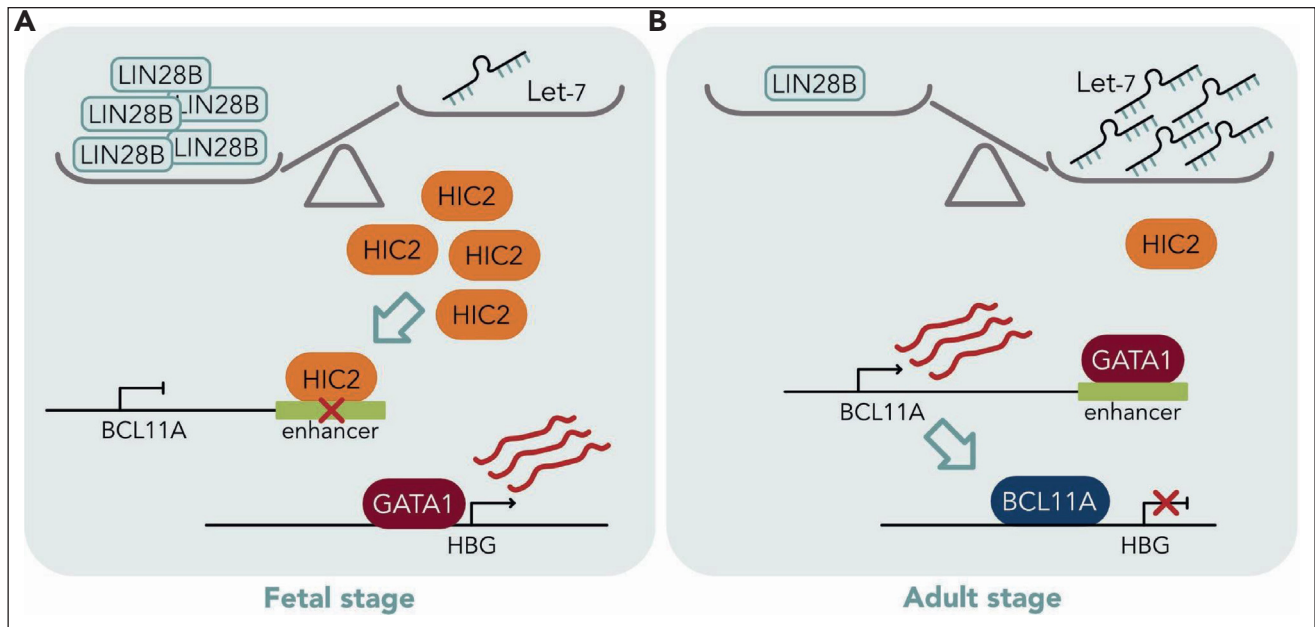
HIC2 links LIN28B/*let-7* to HBG transcription. (A) The balance depicts abundance of RNA binding protein LIN28B in fetal cells resulting in blocked *let-7* miRNA biogenesis. HIC2 can then inactivate the *BCL11A* enhancer, allowing transcription of *HBG* and HbF production. (B) In adult cells, LIN28B is low and *let-7* is abundant, binding to the 3′ UTR of *HIC2* and leading to its degradation. Now, GATA1 can occupy the *BCL11A* enhancer, *BCL11A* is activated and then the protein silences *HBG*. Professional illustration by Somersault18:24.

BCL11A and *HBG* transcriptional regulation (see figure).

Is HIC2 the only relevant *let-7a/f* target in the pathway to *HBG* transcriptional control? Chromatin structure analyses are supportive of this hypothesis. In agreement with the few gene expression changes in the let-7 inhibition model, there were relatively few changes observed using assay for transposase-accessible chromatin (ATAC)-sequencing. Interestingly, HIC2 and GATA binding motifs were enriched among the peaks that lost accessibility, consistent with common targets. Globally, the sites that lost accessibility correlated with increased HIC2 signal and decreased GATA1 signal. The *BCL11A* enhancer exemplifies this exchange. Increased HIC2 signal and decreased GATA1 signal at the enhancer correlated with decreased long-range interactions with the *BCL11A* promoter and decreased transcription.

In a final experiment to clinch that HIC2 critically connects *let-7* to *HBG*, Huang et al depleted HIC2 in *let7a/f*-inhibited HUDEP2 cells. BCL11A was restored to levels in *let-7a/f*-inhibited cells alone and *HBG* was resilenced. The present report connects the dots between *let-7* miRNA and *HBG*, showing that HIC2 is targeted

for degradation by *let-7*, and supplies a satisfying explanation to the proposal of the Miller group that small RNAs have a central role in globin gene switching. The miRNA pathway provides a so far underexplored regulatory option for augmenting fetal hemoglobin.

Conflict-of-interest disclosure: A.D. declares no competing financial interests. ■

REFERENCES

1. Huang P, Peslak SA, Shehu V, et al. *let-7* miRNAs repress HIC2 to regulate BCL11A transcription and hemoglobin switching. *Blood.* 2024;143(19): 1980-1991.

2. Liu N, Hargreaves VV, Zhu Q, et al. Direct promoter repression by BCL11A controls the fetal to adult hemoglobin switch. *Cell.* 2018; 173(2):430-442.e17.

3. Martyn GE, Wienert B, Yang L, et al. Natural regulatory mutations elevate the fetal globin gene via disruption of BCL11A or ZBTB7A binding. *Nat Genet.* 2018;50(4):498-503.

4. Bauer DE, Kamran SC, Lessard S, et al. An erythroid enhancer of BCL11A subject to genetic variation determines fetal hemoglobin level. *Science.* 2013;342(6155):253-257.

5. Huang P, Peslak SA, Ren R, et al. HIC2 controls developmental hemoglobin switching by repressing BCL11A transcription. *Nat Genet.* 2023;55(9):1608.

6. Bartel DP. Metazoan microRNAs. *Cell.* 2018; 173(1):20-51.

7. Lee YT, de Vasconcellos JF, Yuan J, et al. LIN28B-mediated expression of fetal hemoglobin and production of fetal-like erythrocytes from adult human erythroblasts ex vivo. *Blood.* 2013;122(6):1034-1041.

https://doi.org/10.1182/blood.2024024191

THROMBOSIS AND HEMOSTASIS

Comment on Arce et al, page 1992

Taking AIM

Thomas A. J. McKinnon | Imperial College London

In this issue of *Blood*, Arce and colleagues present an elegant study showing that the autoinhibitory module (AIM) of von Willebrand factor (VWF) may be targeted to either be activated or inhibited.[1] The VWF A1 domain contains the binding site for platelet glycoprotein Ib-alpha (GPIb) and this represents

the initial port of interaction for circulating platelets and VWF at sites of injury.[2] Recent work has demonstrated that the 2 proline and O-linked glycan-rich regions that exist on either side of the VWF A1 domain cooperate to control access of GPIb to its binding site.[3-5] These have been termed the N-terminal and C-terminal AIM (N-AIM and C-AIM, respectively).

In their study, Arce et al generated nanobodies against a VWF A1 protein containing both AIM sequences. Next, they selectively sorted the nanobodies to isolate specific binders to the 2 AIM portions. Three nanobodies, 6C4, 6C11, and 6D12, induced platelet activation and binding to GPIb similar to ristocetin, indicating activation of VWF. These 3 nanobodies all bound to the N-AIM with high (nanomolar) affinity and, very interestingly, 6D12 recognized an epitope in the N-AIM that includes the crucial O-linked glycans.[6,7] Finally, for this part of the study, the authors used hydrogen-deuterium exchange to demonstrate that 6D12 binds to the N-AIM and increases accessibility of the GPIb binding site. In addition to providing useful information on how the N-AIM functions, these activating nanobodies may well prove to be valuable research tools. Because they behave similarly to ristocetin, these nanobodies may be useful in diagnostic testing for VWF by overcoming some of the pitfalls associated with ristocetin, such as the P1467S mutation that prevents ristocetin binding.[8]

Arce and colleagues also investigated nanobodies against the C-AIM and identified 2 clones: Nd4 and Nd6. In contrast to the N-AIM nanobodies, Nd4 and Nd6 both inhibited platelet aggregation and, moreover, inhibited VWF-mediated platelet capture under arterial shear stress. The authors then solve the crystal structure of the VWF-A1 domain in complex with Nd6, with some stunning results. The Nd6 clone interacted with the C-AIM regions with some physical distance away from the A1 domain; furthermore, for the first time, the structure was found to resolve one of the O-linked N-acetylgalactosamine residues at position 1468. Most strikingly, it may be first time this structure demonstrated strong evidence of an interaction between N-AIM and C-AIM. From the resolved residues, both AIM modules pointed away from the A1 domain and cooperated to form the entire AIM module that controlled access to the GPIb binding site.

This important study sheds further light on how the VWF A1 domain engages with GPIb and the intricate molecular process that prevents aberrant platelet binding while allowing the VWF molecule to respond to shear forces and promote platelet binding. Although targeting the VWF A1 domain for antithrombotic therapy is not new, understanding how we can selectively target this region without drastic compromise of function may lead to novel and improved anti-VWF targeting agents. This is certainly something to AIM for.

Conflict-of-interest disclosure: The author declares no competing financial interests. ∎

REFERENCES

1. Arce NA, Markham-Lee Z, Liang Q, et al. Conformational activation and inhibition of von Willebrand factor by targeting its autoinhibitory module. *Blood*. 2024;143(19):1992-2004.

2. Sadler JE. Biochemistry and genetics of von Willebrand factor. *Annu Rev Biochem*. 1998;67:395-424.

3. Arce NA, Cao W, Brown AK, et al. Activation of von Willebrand factor via mechanical unfolding of its discontinuous autoinhibitory module. *Nat Commun*. 2021;12(1):2360.

4. Deng W, Wang Y, Druzak SA, et al. A discontinuous autoinhibitory module masks the A1 domain of von Willebrand factor. *J Thromb Haemost*. 2017;15(9):1867-1877.

5. Zhao YC, Wang H, Wang Y, Lou J, Ju LA. The N-terminal autoinhibitory module of the A1 domain in von Willebrand factor stabilizes the mechanosensor catch bond. *RSC Chem Biol*. 2022;3(6):707-720.

6. Nowak AA, Canis K, Riddell A, Laffan MA, McKinnon TA. O-linked glycosylation of von Willebrand factor modulates the interaction with platelet receptor glycoprotein Ib under static and shear stress conditions. *Blood*. 2012;120(1):214-222.

7. Canis K, McKinnon TA, Nowak A, et al. The plasma von Willebrand factor O-glycome comprises a surprising variety of structures including ABH antigens and disialosyl motifs. *J Thromb Haemost*. 2010;8(1):137-145.

8. Flood VH, Friedman KD, Gill JC, et al. Limitations of the ristocetin cofactor assay in measurement of von Willebrand factor function. *J Thromb Haemost*. 2009;7(11):1832-1839.

https://doi.org/10.1182/blood.2024024034

THROMBOSIS AND HEMOSTASIS

Comment on Kumar et al, page 2005

Prothrombin forced into an awkward position

Rolf T. Urbanus | University Medical Center Utrecht

In this issue of *Blood*, Kumar et al use a model antibody to show that a subpopulation of antiprothrombin antibodies found in people with antiphospholipid syndrome act as anticoagulants by stabilizing prothrombin into a conformation that limits its activation by the prothrombinase complex.[1]

Diagnosis of the rare autoimmune disorder antiphospholipid syndrome requires the persistent presence of antiphospholipid antibodies in people with thrombosis or pregnancy-associated morbidity. Thrombotic risk is estimated with antibody profiles based on 3 different antiphospholipid antibodies: antibodies that cause prolongation of clotting time in sensitive clotting assays, so-called lupus anticoagulant, antibodies against the plasma protein β2-glycoprotein I, and antibodies against the phospholipid cardiolipin.[2] Of these 3 antiphospholipid antibodies, only lupus anticoagulant is independently associated with increased risk of thrombosis or pregnancy morbidity. Thrombotic risk is highest in people who are triple positive (ie, positive for anti–β2-glycoprotein I and anti-cardiolipin antibodies as well as lupus anticoagulant).[2]